AIMS Materials Science, 13(5): 1047–1067.
DOI: 10.3934/matersci.2026049
Received: 20 August 2026
Revised: 18 October 2026
Accepted: 06 November 2026
Published: 18 November 2026

https://www.aimspress.com/journal/Materials

Research article

Ferrochrome slag and gamma irradiation for enhanced cement concrete performance

Gonzalo Martínez-Barrera[1,*], Miguel Martínez-López[2], Víctor Varela-Guerrero[3], Joel Olaf Camacho-Gutiérrez[1] and Cynthia Castro-López[1]

[1] Facultad de Química, Universidad Autónoma del Estado de México, Km.12 de la carretera Toluca-Atlacomulco, San Cayetano 50200, México
[2] División de Ingeniería Industrial e Ingeniería en Energía y Desarrollo Sostenible, Universidad Politécnica del Valle de Toluca, Carretera Toluca-Almoloya de Juárez km. 5.6, Almoloya de Juárez 50904, México
[3] Centro Conjunto de Investigación en Química Sustentable UAEM-UNAM, Carretera Toluca-Atlacomulco Km 14.5, Toluca 50200, México

* **Correspondence:** Email: gonzomartinez02@yahoo.com.mx; Tel: +52-55-5184-3931.

Abstract: To reduce the environmental impact of ferrochrome (FeCr) slag waste while providing a sustainable management alternative, this byproduct can be incorporated as an alternative fine aggregate in concrete production. In this study, concrete mixtures were prepared using cement, gravel, and either marble or mine sand as fine aggregates. The fine aggregates were partially replaced with ferrochrome slag in proportions ranging from 10% to 30% by weight. Subsequently, the resulting concrete samples were subjected to gamma irradiation at a dose of 300 kGy. The results demonstrated that the incorporation of 30% by weight of FeCr slag increased the compressive strength by up to 27% in concrete based on marble, and by 28% in concrete based in mine sand. Furthermore, gamma irradiation increased the compressive strength, particularly those containing 30 % by weight of FeCr slag. In these formulations, approximate increases of 20% and 11% were observed in the marble-based and mine sand-based concretes, respectively. These improvements are attributed to radiation-induced modifications in the structural and morphological characteristics of the marble, mine sand, and ferrochrome slag, as confirmed through crystalline phase analysis via X-ray diffraction (XRD), scanning electron microscopy (SEM), and energy-dispersive X-ray spectroscopy (EDS).

Keywords: concrete; ferrochrome slag; gamma radiation; compressive strength; marble; mine sand

1. Introduction

Ferrochrome (FeCr) is produced via a carbothermic process from chromium oxide ore using coke as a reducing agent in electric arc furnaces at 1700 °C. The production of high-carbon ferrochrome generates large quantities of slag waste, which contains traces of heavy metals, such as 65% chromium by weight. As is well known, Cr(VI) is toxic to humans and, depending on its particle size, readily becomes airborne and is inhaled by living organisms, which can be harmful to health at certain concentrations, causing cancer. Therefore, it is advisable to isolate and stabilize it, for example, using a binder such as cement. FeCr slag has a similar size to the coarse aggregates used in concrete, so it can be used in construction materials and promote sustainability. Among other advantages, it can provide increased compressive strength, fluidity, workability, and durability of the concrete, as well as reduced porosity and permeability.

The addition of ferrochrome slag to concrete improves its properties. For example: (a) mechanical characteristics increase as the concentration of FeCr slag increases, due to the rougher surface of FeCr, which contains microcavities. This enables high water absorption and a lower amount of free water in the concrete, thus reducing the effective water/cement ratio. The mechanical interlocking with the cement paste is responsible for the mechanical improvement of the concrete [1]. (b) During concrete production, FeCr slag partially replaced the crushed limestone; the rough surfaces of the aggregates are coated by the cement paste, producing reactions between them and developing strong interfacial bonds and anchorages, consequently improving mechanical performance [2]. (c) Lower permeability and water absorption were obtained after increasing the FeCr slag content [3]. (d) Compressive strength increases with FeCr slag content; the highest values were obtained with 100% by weight of FeCr slag. Furthermore, energy consumption was reduced by 5% [measured by embodied energy (EE)] and CO_2 emissions were reduced by 2.5% [measured by embodied carbon dioxide emissions (ECO_2e) [4,5]. (e) The ultrasonic pulse velocity (UPV) through the concrete increased as the FeCr slag content increased; the highest UPV values were obtained with 40% by weight of FeCr, which was 12% higher than the control concrete. Furthermore, the percentage of water absorption was almost constant after the addition of FeCr [6,7]. Information on these reference works [1–7] is summarized in Table 1.

In contrast, the mechanical properties of concrete decreased slightly when 10–50 wt% of natural sand was replaced with FeCr slag. Specifically, flexural strength, compressive strength, modulus of elasticity, and splitting tensile strength decreased by 9%, 14%, 9%, and 12%, respectively [8]. Similarly, replacing the fine aggregate with FeCr slag resulted in a 3% reduction in compressive strength [6].

FeCr slag has also been incorporated into cement mortars, building bricks, and pavements. In cement mortars, its effects are generally consistent with those observed in concrete. For example, replacing 50% of the silica sand with FeCr slag (0.06–2.36 mm) increases the flexural and compressive strengths by 57% and 34%, respectively. Furthermore, its thermal conductivity increases up to 42%, while capillary water absorption decreases by up to 22%. These improvements are due to the interactions between the cement matrix and the FeCr grains [9]. However, when FeCr slag particles (<1 μm) are added to replace between 25% and 50% by weight of the cement in mortars, the compressive strength decreases up to 29% compared to the control mortar [10].

Table 1. Enhancement of mechanical properties through ferrochrome slag.

FeCr	FeCr size, mm	Compressive strength, MPa (improvement, %)	Flexural strength, MPa (improvement, %)	Tensile splitting strength, MPa (improvement, %)	Elasticity modulus, GPa (improvement, %)	Ref.
22–46 wt%	4	66.3 (25%)	13.5 (32%)	4.8 (12%)	39 (14%)	[1]
25–100 wt%	0.1–10	51 (12%)	6.4 (20%)	3.75 (7.5%)	40 (11.7%)	[2]
20–40 wt%	-	42.9 (23%)	-	-	-	[3]
20–100 wt%	8–20	37.2 (21%)	-	-	-	[4]
50–100 wt%	20	67 (4%)	-	-	-	[5]
25–75 vol%	2.36–16	32 (6%)	-	5.3 (3%)	36.8	[6]
5–40 vol%	-	48 (21%)	5.2 (9%)	3.6 (50%)	-	[7]

In [11], aggregates in the concrete mixes were partially replaced with ferrochrome slag at levels up to 30% by weight. The results indicate that the addition of 10% by weight of ferrochrome increases compressive by 7%, while a 30% by weight of ferrochrome yields compressive strength comparable to the control concrete. Conversely, increasing the ferrochrome slag concentration progressively reduced flexural strength, culminating in a 21% decrease at the 30% replacement level. In [12] study, the aggregates in the manufactured concrete were partially replaced with ferrochrome slag at 50%, 75%, and 100% by weight. The results indicate that the highest compressive strength values were obtained with 75% by weight of ferrochrome added, representing a 5.2% increase compared to the control concrete. Regarding flexural strength, a decrease was observed at ferrochrome concentrations of 50% and 100%. In [13], sustainable concretes were produced by partially replacing fine aggregates with ferrochrome slag up to 60% by weight. The results indicate a slight increase of 1.5% in compressive strength at a ferrochrome content of 40% by weight. Flexural strength shows a similar trend, with a slight increase at a ferrochrome concentration of 40% by weight. Moreover, in [14], concrete specimens were manufactured by replacing natural aggregates with ferrochrome slag in proportions of 20%, 50%, 75%, and 100% by volume. The results showed that the concrete density increased by up to 13% with a 100% ferrochrome slag substitution. Flexural strength was 11% higher with a 50% ferrochrome slag content than that of the control concrete.

Moreover, in [15], high-performance, environmentally friendly concrete was produced by replacing sand with ferrochrome slag up to 100% by weight. The results show that the concrete density gradually increases as the amount of ferrochrome slag increases. Furthermore, the compressive strength, assessed at 180 days, increases by up to 22% with a 100% ferrochrome content. In building bricks, 10–30 wt% of the clay was replaced with FeCr slag particles (<100 μm). This substitution reduced the flexural and compressive strengths by 45% and 21.2%, respectively, while increasing the thermal conductivity by 5.4% compared with the control bricks [16]. In the manufacture of flexible pavements, ferrochrome slag particles (<25 mm) enabled resilient modulus (Mr) values of 200 to 500 MPa, deformations of up to 3.5 mm and Poisson coefficients of 0.21 to 0.36 [17].

Regarding the effects of gamma-ray irradiation on concrete or cement paste, in hardened cement paste subjected to an irradiation dose of 5×10^4 kGy, changes in physical properties occur, and a significant improvement in flexural strength is observed, accompanied by the formation of aragonite (orthorhombic $CaCO_2$) and vaterite (hexagonal $CaCO_3$); the latter contributes to the

strengthening of the C–S–H structure through pseudomorphs [18]. From a physicochemical perspective, gamma irradiation can induce ionization and electronic excitation in cementitious materials. Radiolysis of water can generate reactive species in the pore solution, which can participate in subsequent chemical reactions involving dissolved species and cement hydration products [19]. Radiation-induced point defects have also been detected in silica-based materials using electron paramagnetic resonance spectroscopy [20]. Irradiated cementitious materials have shown varying responses in mineral composition, porosity, and mechanical performance, highlighting the importance of dose, material composition, and environmental conditions [21,22].

In the case of irradiated concrete, the pore fluid within the material is affected by radiolysis. The radiolysis of water generates hydrated electrons (e^-_aq) and hydrogen peroxide (H_2O_2), which act, respectively, as reducing agents for dissolved oxygen (O_2) and as precursors for its formation. The depletion of O_2 is due not only to its rapid reaction with hydrated electrons but also to processes involving trapped peroxide species. Calcium peroxide octahydrate (CaO_2•$8H_2O$) forms through reactions involving dissolved calcium, portlandite, and ettringite. However, since this compound is unstable, it disappears from the cement paste once H_2O_2 is no longer in the surrounding medium [19]. As for neutron irradiation in reinforced concrete, an increase in neutron fluence leads to an increase in the yield strength of the reinforcing steel, as well as in the load-bearing capacity of structural elements that fail in tension. Conversely, the load-bearing capacity of elements that fail in compression decreases, and the energy dissipation capacity is significantly reduced. Furthermore, in the context of the long-term operation of nuclear power plants, this phenomenon should be considered a form of aging-related damage [23].

Ferrochrome slag has also been investigated as a radiation-shielding material. For example, in [24], bricks in which 10–30 wt% of the clay was replaced with FeCr slag particles (<100 μm) were exposed to neutron irradiation. The results showed a 26% reduction in compressive strength compared with the control bricks. In contrast, flexural strength and water absorption exhibited a non-monotonic trend: both properties decreased at 10 wt% FeCr slag, increased at 20 wt%, and decreased again at 30 wt% replacement. Flexural strength increased up to 98%, and water absorption by 9%. In [25], composite materials produced with epoxy resin and 50–80 wt% FeCr slag were exposed to gamma rays. The results show that the linear attenuation coefficient (μ) increases up to 116%. However, the absorbed dose decreases with increasing FeCr slag concentrations, becoming up to 12% lower.

In this study, concrete mixtures were prepared using cement, gravel, and either marble or mine sand as the fine aggregate. The fine aggregate was partially replaced with ferrochrome slag at replacement levels of 10–30 wt%. The resulting concretes were subsequently exposed to gamma irradiation at a dose of 300 kGy. The influence of FeCr slag incorporation and gamma irradiation on the concrete was evaluated through compressive strength testing, complemented by X-ray diffraction (XRD), scanning electron microscopy (SEM), and energy-dispersive X-ray spectroscopy (EDS) analyses to characterize the corresponding structural, microstructural, and compositional changes.

2. Materials and methods

2.1. Materials

The particle size distribution of the gravel was determined by sieve analysis using sieves with 3/4", 3/8", and 1/4" openings, according to standard NMX-C-077-ONNCCE-2004. The material retained on each sieve was then weighed. The gravel particles retained on the 1/4" (6.3 mm) sieve were selected for concrete preparation, at this fraction showed the highest retention percentage (45%). The resulting particle size distribution of the gravel is presented in Table 2. Furthermore, the density of the gravel was 2.65 g/cm^3 (EN 1097-6 standard).

Table 2. Particle size distribution of gravel.

Sieve	Size, mm	Retained weight, g	Retained weight, %	Retained accumulated weight, %
3/4"	19.0	0	0	0
3/8”	9.5	6,000	44	44
1/4“	6.3	6,200	45	89
Pan	-	1,500	11	100

The marble, with a composition of 90% calcite ($CaCO_3$) and 10% dolomite [$CaMg(CO_3)_2$], was donated by Company Minerales GOSA S.A., located in Atizapán de Zaragoza, México. The data provided on its properties are shown in Table 3.

Table 3. Properties of marble.

Property	Value
Density, g/cm^3	2.93
Particle size, mm	0.6
Mohs hardness	3–4
Compressive strength, MPa	58–98
Tensile strength, MPa	10–35
Melting point, °C	825

The mine sand had an average diameter of 3.0 mm (mesh 50), a density of 2.53 g/cm^3 (EN 1097-6 standard) and a melting point of 1,600 °C.

The ferrochrome slag was supplied by Eti-Krom-Works (Elazıg, Turkey) and processed by grinding and crushing. Its physicochemical characteristics are shown in Table 4, while its chemical composition is reported in Table 5 [16].

These dimensions were selected for coarse and fine aggregates to avoid problems with homogeneity and workability. It is known that fine aggregates with the appropriate fineness improve the workability of concrete and contribute to greater mechanical strength.

Table 4. Physicochemical characteristics of ferrochrome slag [16].

Property	Value
Density, g/cm^3	2.93
Particle size, mm	0.15
Color	Gray
Apparent density, g/cm^3	3.2–3.7
Specific density	7.3–7.5
Melting temperature, °C	1,550–1,650

Table 5. Chemical composition of ferrochrome slag [16].

Compound	Composition, %
MgO	38.5
SiO_2	29.38
Al_2O_3	23.47
Cr_2O_3	5.17
Fe_2O_3	1.55
CaO	0.93
Na_2O	0.15
K_2O	0.06

2.2. Concrete production

Cylindrical control concrete specimens (5 cm in diameter × 10 cm in height) were prepared using Type II Portland cement (Cruz Azul^{TM}, Mexico), with 0.15 mm size (sieve 100), gravel, and fine aggregates (marble or mine sand), following the ASTM C31 standard. The mix proportion of cement, gravel, and fine aggregate was 1:2.5:1.5 by weight, and the water/cement ratio was kept constant at 0.65. In addition, potable water was used, free of solid waste and suspended organic matter, and free of fats or oils. Control concrete is designated as C in Table 6.

Table 6. Cement concrete composition.

Cement concrete	Cement, g	Gravel, g	Water, g	Fine aggregate, g	FeCr slag, g	FeCr slag, wt%
C	78.7	196.75	51.15	118.05	0	0
C-10F	78.7	196.75	51.15	106.24	11.80	10
C-20F	78.7	196.75	51.15	94.44	23.60	20
C-30F	78.7	196.75	51.15	82.63	35.40	30

The fine aggregate of the concrete, consisted of marble or mine sand, was partially replaced by ferrochrome slag in proportions of 10% to 30% by weight. The concretes are designated C-10F, C-20F, and C-30F, respectively, in Table 6. The concrete mixtures were cast at room temperature and cured under controlled humidity conditions. Since the specimens were analyzed at different

curing times (7, 14 and 28 days), thirty-six specimens were prepared for each type of formulation, i.e., for concrete with marble or mine sand.

2.3. Irradiation of concrete specimens

After a curing period of 28 days, the four types of concrete samples shown in Table 6 were irradiated with a dose of 300 kGy at a dose rate of 2.5 kGy/h, in an atmosphere air at room temperature. The compressive strength of irradiated concrete was compared with that of non-irradiated concrete, which was subjected to a 28-day curing process and subsequently to 120 h of maintenance in an air atmosphere before performing the mechanical tests.

A dyed polymethyl methacrylate (PMMA) dosimeter was used to determine the absorbed dose. Irradiation was performed in a Transelektro LGI-01 industrial irradiator equipped with Co-60 sources with a half-life of 5.2 years, manufactured by IZOTOP Isotope Institute Co. Ltd., Budapest, Hungary. The irradiator had a chamber containing a ring of fixed cobalt-60 rods, embedded in the main shielding, where the samples were loaded, which were placed in the geometric central ring to ensure homogeneous and high dose exposure to gamma rays.

In a separate study, to study the effects of gamma radiation on marble, mine sand, and ferrochrome slag, these were placed in polyethylene bags (5 × 7 cm) and exposed to gamma radiation at doses of 300 kGy following the same procedure as the concrete specimens. No direct measurements of the sample temperature were performed during irradiation. Therefore, the experimental data obtained in this study did not enable us to determine whether the sample temperature remained constant throughout the exposure process.

2.4. Compressive strength

The compressive strength of the concrete specimens was measured using a Controls^{TM} model 70-S17C2 universal testing machine (Cernusco, Italy) with a load capacity of 30 tons. The tests were conducted at a crosshead displacement rate of 0.3 mm/min in accordance with ASTM C39/C39M-01. The testing age was 28 days with a tolerance of ±20 h, as specified by ASTM C39/C39M-14.

2.5. SEM analysis of fracture surfaces in concrete specimens

The fracture zones of the analyzed samples were examined using SEM with EDS. Five images per sample were analyzed at magnifications of 100×, 500×, 1000×, and 1500×. First, the samples were coated with gold in a Denton Desk IV sputtering chamber. The vacuum system was optimized between 30 and 1,000 mtorr. Subsequently, the samples were observed in secondary electron mode using a JEOL JSM-6510LV scanning electron microscope, operated at an acceleration voltage of 30 kV, with a maximum resolution of 5 nm under high vacuum. The microscope features an attached OXFORD X-ray detector for chemical microanalysis, with a resolution of 137 eV, and operates in low-high vacuum mode.

2.6. XRD analyisis of ferrochrome slag, marble, and mine sand

The crystalline phases were analyzed by powder XRD using a Rigaku Ultima IV diffractometer. The system utilized a copper anode X-ray tube generating Cu $K\alpha_1$ radiation (λ = 1.5406 Å), operated at a voltage of 35 kV and a current of 30 mA. The spectra were obtained by scanning the samples from 10º to 60° (2θ angle), and a rate of 0.5°/min.

3. Results

3.1. Compressive strength of concrete incorporating ferrochrome slag

The compressive strength values of concrete containing ferrochrome slag combined with either marble or mine sand as aggregates are shown in Figure 1. Thirty-six samples were analyzed. For each formulation, the arithmetic mean and standard deviation of the experimental results were calculated. The standard deviation is represented by error bars in the corresponding graphs, and the data for the concrete specimens are presented in Table 7.

Figure 1a shows the results for concrete with marble, designated as C-M in Table 7. It also shows concrete with marble incorporating 10%, 20%, and 30% by weight of ferrochrome slag as aggregate, designated as C-M-10F, C-M-20F, and C-M-30F, respectively. Figure 1b shows the results for concrete with mine sand, designated as C-mS, as well as concrete with mine sand incorporating 10%, 20%, and 30% by weight of ferrochrome slag as aggregate, designated as C-mS-10F, C-mS-20F, and C-mS-30F, respectively, and shown in Table 8.

In the case of concrete incorporating ferrochrome slag combined with marble (Figure 1a), the control concrete cured for 28 days had a value of 21.3 MPa. Compressive strength values increased with curing time, as well as with the content of ferrochrome slag. The highest values were obtained for concrete containing 30% by weight of ferrochrome slag, cured for 28 days, specifically 27.1 MPa, representing a 27% increase compared to the control concrete.

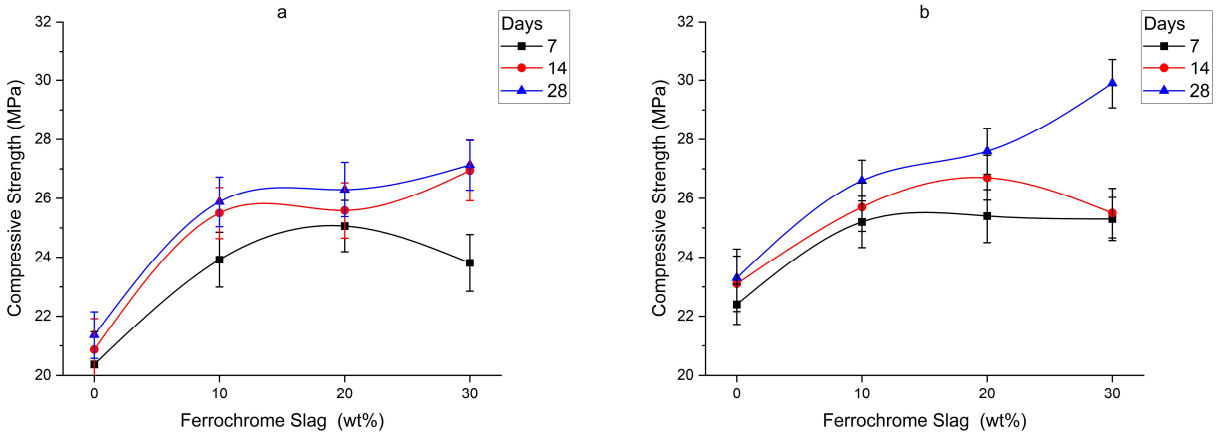


Figure 1. Compressive strength of concrete incorporating ferrochrome slag combined with either (a) marble or (b) mine sand as aggregates.

Table 7. Compressive strength of concrete specimens containing marble.

Concrete	Curing time, days					
	7		14		28	
	Compressive strength, MPa	Standard deviation	Compressive strength, MPa	Standard deviation	Compressive strength, MPa	Standard deviation
C-M	20.3	1.10	20.8	1.05	21.3	0.79
C-M-10F	23.9	0.93	25.5	0.87	25.8	0.84
C-M-20F	25.0	0.87	25.5	0.94	26.3	0.92
C-M-30F	23.8	0.96	26.9	1.02	27.1	0.85

For concretes incorporating ferrochrome slag combined with mine sand (Figure 1b), the control concrete exhibited a compressive strength of 23.3 MPa after 28 days of curing. A similar trend to that of marble-containing concretes was observed: compressive strength increased gradually with curing time and the incorporation of FeCr slag. The highest values were obtained with 30% by weight of FeCr slag and 28 days of curing; specifically, 29.9 MPa, which represented a 28% increase over the control concrete. The standard deviation data for the concrete specimens after 28 days of curing are presented in Table 8. Furthermore, the maximum values recorded for the concretes containing mine sand were 10% higher than those obtained for concretes containing marble; thus, a smaller particle size (0.3 mm for the mine sand) resulted in greater strength compared to the 0.6 mm particle size of the marble.

The mechanical strength of concrete depends on the intrinsic strength of the aggregates and on the strength of the interfacial bond between the cementitious matrix and those aggregates. In this study, the FeCr slag particles exhibited a rough surface morphology, characterized by cavities and microcracks, which facilitated the penetration of cement hydration products into these irregularities. This promoted mechanical interlocking between the slag particles and the cement paste, leading to a stronger interfacial bond and, consequently, higher compressive strength. Based on these, which demonstrated increased compressive strength, the following conditions were selected for the concrete irradiation process: a curing time of 28 days and an irradiation dose of 300 kGy.

Table 8. Compressive strengths of concrete specimens containing mine sand.

Concrete	Curing time, days					
	7		14		28	
	Compressive strength, MPa	Standard deviation	Compressive strength, MPa	Standard deviation	Compressive strength, MPa	Standard deviation
C-mS	22.4	0.68	23.1	0.94	23.3	0.98
C-mS-10F	25.2	0.87	25.7	0.82	26.6	0.69
C-mS-20F	25.4	0.9	26.7	0.76	27.6	0.78
C-mS-30F	25.3	0.73	25.5	0.84	29.9	0.83

3.2. Compressive strength of unirradiated and gamma-irradiated concrete specimens

Figure 2 shows the compressive strength values of the irradiated and non-irradiated concretes. The types of concrete evaluated are shown in Table 9. Two types of non-irradiated concrete were evaluated: concrete with marble and ferrochrome slag, designated C-M-F, and concrete with mine sand and ferrochrome slag, designated C-mS-F. For the irradiated concretes: concrete with marble, ferrochrome slag, and irradiated at 300 kGy, designated C-M-F-300, and concrete with mine sand, ferrochrome slag, and irradiated at 300 kGy, designated C-mS-F-300. In general, a trend toward higher compressive strength following irradiation was observed across all studied FeCr concentrations (Table 9). However, no substantial changes in this property were evident in the C-M-F; the non-irradiated samples exhibited a value of 21.3 MPa, while after irradiation, this value remained very similar, at 21.5 MPa. Therefore, gamma irradiation did not significantly affect the mechanical strength of these concretes. In contrast, for the C-mS-F, the compressive strength increased from 23.3 MPa to 24.1 MPa following irradiation, representing an improvement of approximately 3.4%. This increase could be attributed to the interaction between gamma radiation and the chemical components of the mine sand, which may promote stronger interactions between the aggregate particles and the cement paste, resulting in better mechanical performance.

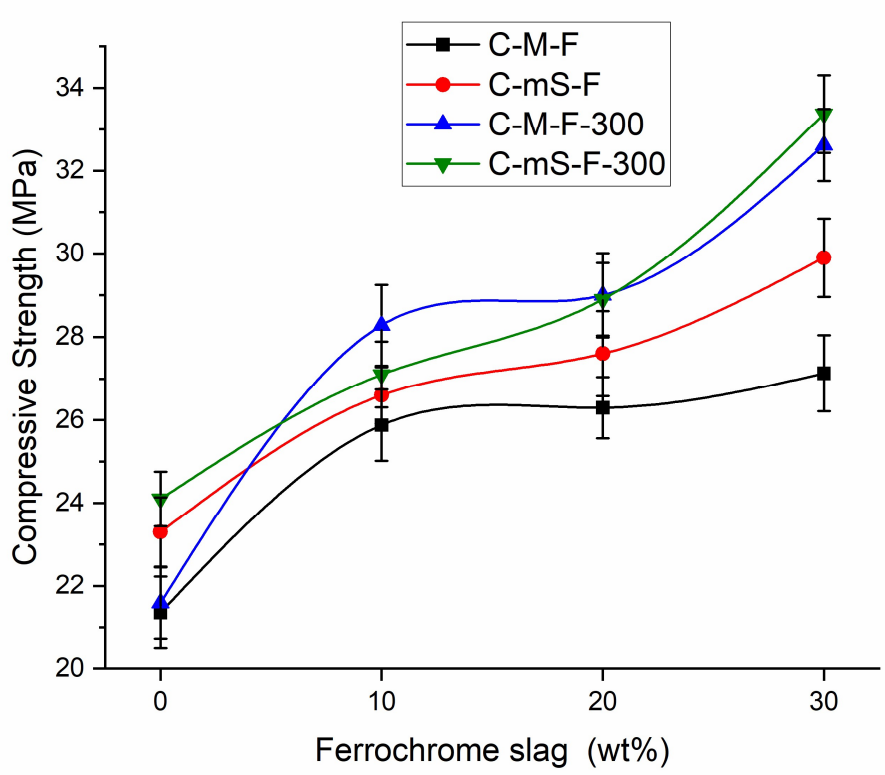


Figure 2. Compressive strength of unirradiated and gamma-irradiated concrete incorporating ferrochrome slag combined with either marble or mine sand.

The C-M-F-300 achieved strength of 32.6 MPa, representing a 20% improvement over the C-M. Moreover, the C-mS-F-300 reached 33.3 MPa, representing an 11% improvement compared to the C-mS. The combination of a high FeCr slag content and a high irradiation dose resulted in greater compressive strength. This improvement can be attributed to the effects of gamma irradiation on

cement hydration products, whose chemical components may interact with the elements present in the fine aggregates (marble and mine sand). Such interactions promote a stronger bond between the cement matrix and the aggregates, which translates into better mechanical performance.

Table 9. Compressive strength of unirradiated and gamma-irradiated concrete specimens.

Concrete	Ferrochrome slag, wt%							
	0		10		20		30	
	Compressive strength, MPa	Standard deviation	Compressive strength, MPa	Standard deviation	Compressive strength, MPa	Standard deviation	Compressive strength, MPa	Standard deviation
C-M-F	21.3	0.87	25.8	0.86	26.3	0.74	27.1	0.91
C-mS-F	23.3	0.84	26.6	0.68	27.6	1.02	29.9	0.94
C-M-F-300	21.5	0.86	28.2	0.97	29.0	1.01	32.6	0.87
C-mS-F-300	24.1	0.66	27.1	0.79	28.9	0.87	33.3	0.94

3.3. Morphology of concrete specimens

3.3.1. Concrete containing marble

SEM images of the fractured concrete surfaces are presented in Figure 3. The C-M exhibited an irregular and rough morphology, with particle sizes ranging from 2 to 20 μm (Figure 3a). In contrast, the C-M-F displayed a rougher surface morphology with smaller particle sizes, varying between 1 to 10 μm (Figure 3b). Following gamma irradiation, notable changes were observed in the concrete: a smoother and more compact surface with irregular particles (2–10 μm) (Figure 3c). This is because the FeCr particles have a rough surface with microcavities, which enables high water absorption. Consequently, the amount of free water in the concrete mixture is reduced, leading to a lower effective water/cement ratio. This promotes greater mechanical interlocking between the aggregate particles and the cement paste, which contributes to an improvement in the mechanical performance of the concrete.

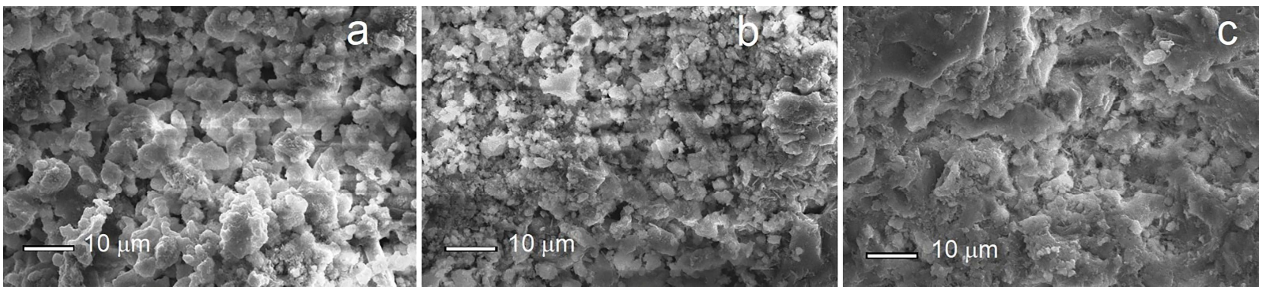


Figure 3. SEM images of fractured concrete surfaces: (a) C-M; (b) C-M-F; and (c) C-M-F-300.

The elemental composition of the concretes C-M, C-M-F, and C-M-F-300, is presented in Figure 4. The main elements detected were oxygen (45.4%–50.3%), calcium (24.4%–29.5%), carbon (8.1%–11.9%), and silicon (7.4%–8.2%). Following gamma irradiation, the measured calcium content decreased 20%, whereas the carbon and silicon contents increased by 38% and 11%,

respectively. These variations indicate changes in the relative elemental composition of the analyzed concrete specimens after irradiation. However, because EDS results are generally expressed as relative elemental percentages, these changes do not necessarily demonstrate actual elemental loss or gain or confirm chemical interactions among the constituents.

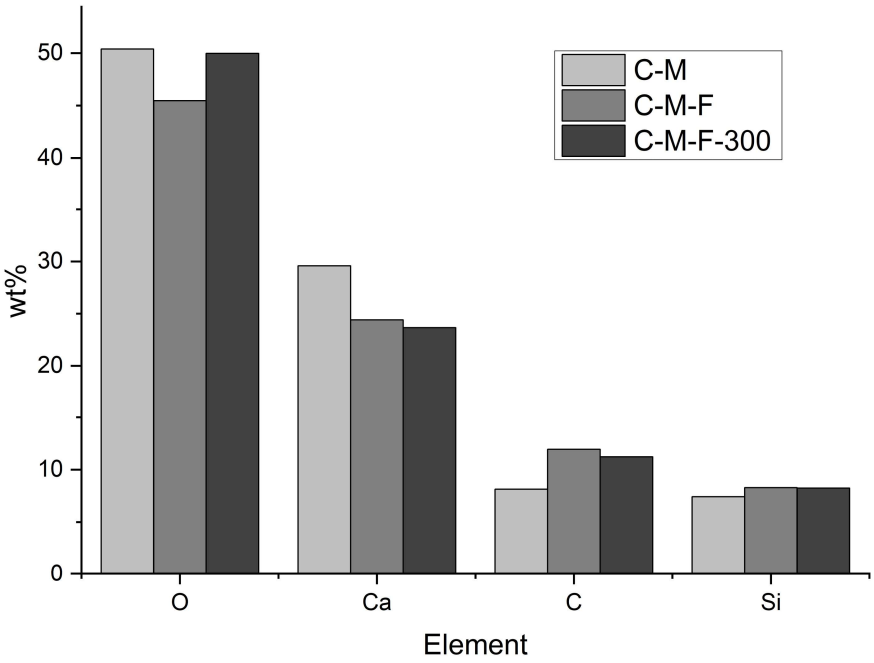


Figure 4. Chemical composition of unirradiated and gamma-irradiated concretes containing marble and ferrochrome slag.

Lower concentrations of Mg, Al, Fe, and Cr were detected in the concrete samples, as shown in Figure 5. Magnesium was not detected in the C-M; however, its concentration reached 3.18 wt% following the incorporation of ferrochrome slag and decreased to 2.92 wt% after gamma irradiation. Aluminum concentrations increased from 1.41 wt% in the marble-based concrete to 3.04 wt% after FeCr slag incorporation, then decreased to 2.52 wt% following irradiation. These variations may reflect differences in the elemental composition and microstructure of the concrete matrix. However, further analyses are required to establish whether irradiation-induced chemical interactions involving aluminum occurred.

The iron concentration decreased from 1.59 wt% to 0.81 wt%, representing a reduction of approximately 49%. Similarly, chromium was not detected in the C-M; whereas its concentration decreased from 0.83 wt% in the FeCr-containing concrete to 0.66 wt% after irradiation. The observed decreases in magnesium, aluminum, iron, and chromium concentrations following irradiation may be associated with changes in the microstructure or in the relative distribution of the elements within the analyzed regions. Nevertheless, these variations should be interpreted cautiously, as changes in elemental percentages obtained by EDS do not necessarily indicate actual elemental loss or chemical transformation.

EDS measurements revealed differences in the relative elemental proportions among the examined marble-based concrete samples, including variations in Ca, Si, Fe, and Cr. These differences characterize the local composition of the analyzed regions on the fracture surface. Given

that concrete is a heterogeneous, multiphase material, the measured elemental proportions may depend on the specific region analyzed and the local surface topography. Consequently, the results obtained via EDS are interpreted as localized compositional measurements rather than as direct evidence of changes in the material's overall composition. Quantitative comparisons should be evaluated by taking into account the acquisition and quantification procedures, as well as the spatial representativeness of the analyzed regions. Furthermore, the observed variations cannot be attributed exclusively to gamma irradiation.

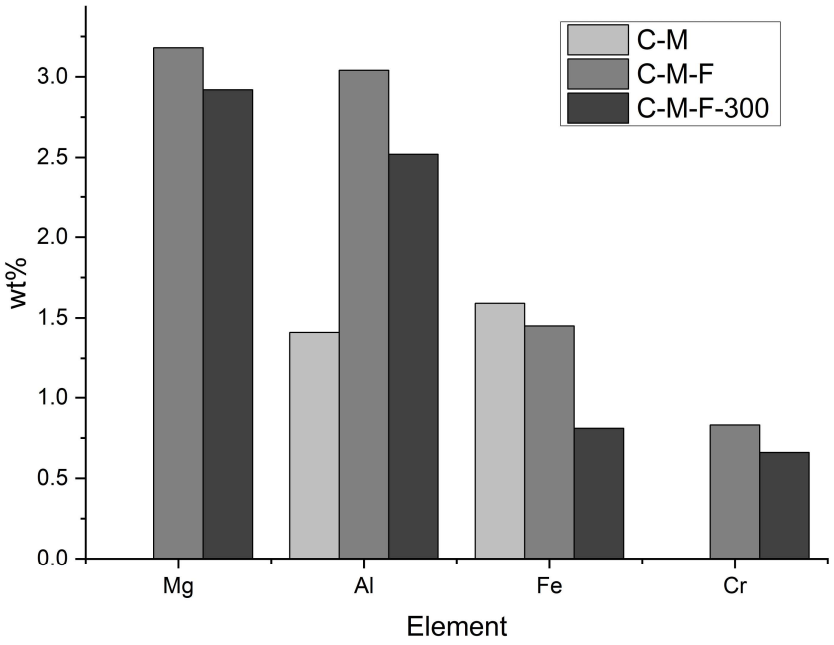


Figure 5. Chemical composition of concrete containing marble, ferrochrome slag, and gamma-irradiated materials.

3.3.2. Concrete containing mine sand

SEM images of the fractured concrete surfaces are presented in Figure 6. The C-mS exhibits a relatively rough surface characterized by irregular particles ranging from 2 to 10 μm and flat structures measuring 2–30 μm (Figure 6a). In contrast, the C-mS-F displays a comparatively smoother surface, with fewer irregular particles smaller than 10 μm (Figure 6b). Following gamma irradiation, noticeable microstructural changes are observed in the C-mS-F-300, including surface roughness, a broader distribution of irregular particle sizes, and the formation of microcracks (Figure 6c). These observations suggest that incorporating ferrochrome slag and applying gamma irradiation are associated with changes in the fracture-surface morphology of the concrete.

Figure 7 presents the elemental composition of concretes C-mS, C-mS-F, and C-mS-F-300. Oxygen was the most abundant element, accounting for 49.2% - 50.8%, followed by calcium (17.0%–19.5%), silicon (12.3%–13.6%), and carbon (9.8%–11.1%). The concentrations of these major elements exhibited relatively small variations among the three concrete formulations, with changes not exceeding 14.4%. These results suggest that incorporating ferrochrome slag and applying gamma irradiation at 300 kGy did not substantially alter the overall proportions of the major elements detected.

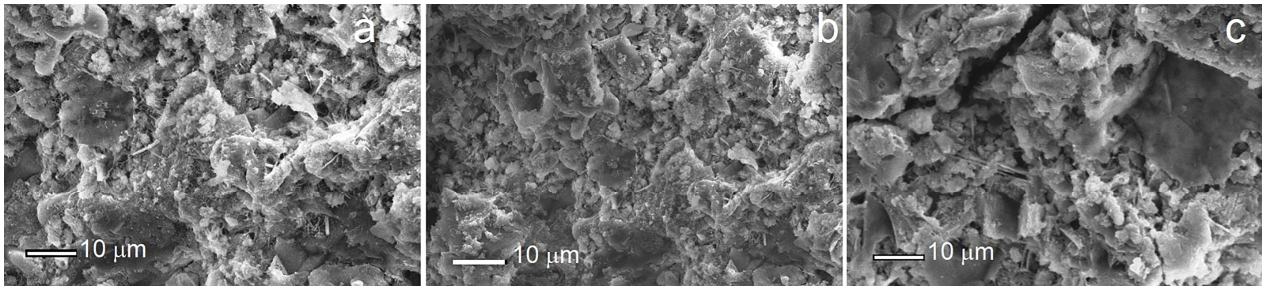


Figure 6. SEM images of fractured concrete surfaces: (a) C-mS; (b) C-mS-F; and (c) C-mS-F-300.

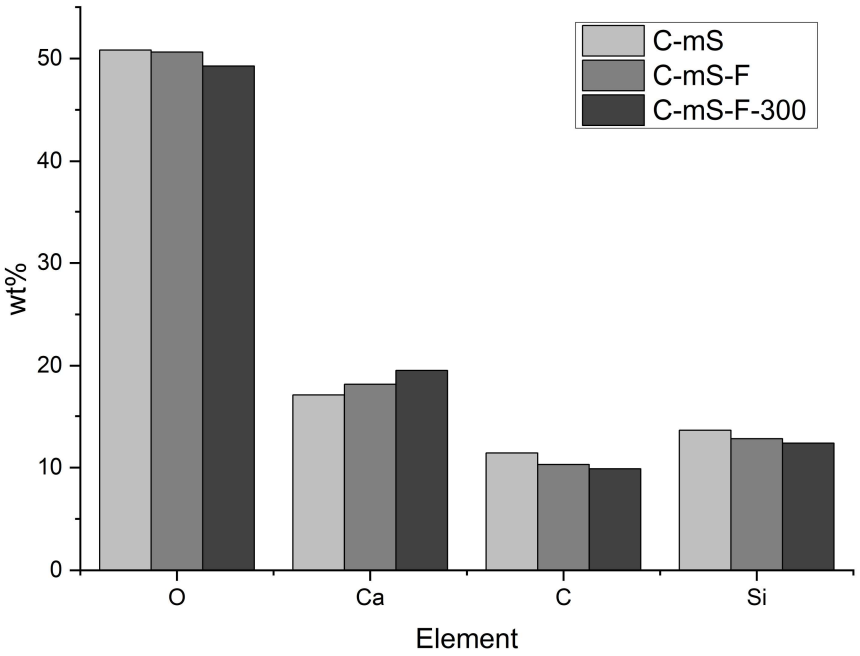


Figure 7. Chemical composition of concrete containing mine sand, ferrochrome slag, and gamma-irradiated materials.

Low percentages were obtained for the elements Mg, Al, and Fe (Figure 8). Magnesium was not present in concrete with mine sand, while the percentages of aluminum increased from 3.0 wt% to 3.6 wt%, representing a 20% improvement. A similar trend was observed for iron, which increased from 1.6 wt% to 1.9 wt%, representing an 18% increase. No chromium was detected in the C-mS and C-mS-F. This finding differs from the results obtained for the C-M-F, in which chromium was detected. Given that the available measurements do not enable determination of the cause of this difference, the failure to detect chromium in the C-mS should not be interpreted as proof of its total absence from the material.

In the case of concrete specimens based on mine sand, the EDS results showed differences in the relative proportions of the detected elements, including Al and Fe. These observations describe the elemental composition of the analyzed regions, but they do not establish that gamma irradiation caused an increase in the absolute content of these elements. Likewise, the absence of a detectable Cr signal in the analyzed regions should not be interpreted as proof of the total absence of chromium in the specimens.

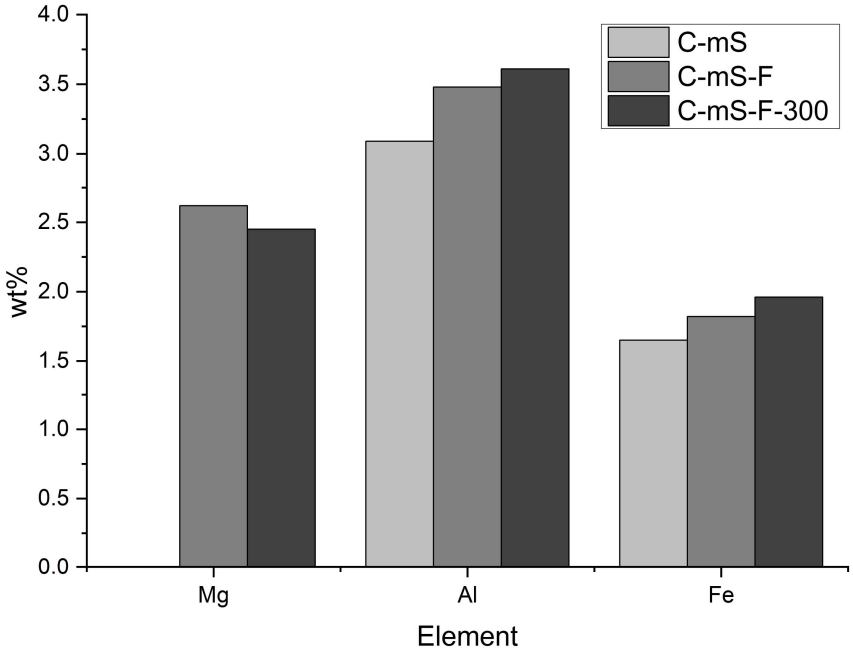


Figure 8. Chemical composition of concrete containing mine sand, ferrochrome slag, and gamma-irradiated materials.

3.4. XRD analysis of mineral aggregates

The compressive strength of concrete depends partly on the mechanical properties of its aggregates, which are related to their mineralogical composition and microstructure. To investigate the effects of gamma irradiation on these characteristics, the crystalline phases of marble, mine sand, and ferrochrome slag were evaluated before and after irradiation using XRD.

Figure 9 compares the XRD patterns of non-irradiated and gamma-irradiated marble. Four prominent diffraction peaks corresponding to calcite ($CaCO_3$), labeled C, were identified at 2θ = 29.64°, 43.24°, 47.62°, and 48.58°. Two additional peaks associated with dolomite [$CaMg(CO_3)_2$], labeled D, were observed at 2θ = 36.04° and 56.62°. The diffraction peak positions remained unchanged following gamma irradiation, indicating that no detectable changes in the crystalline phases occurred. However, the irradiated samples exhibited lower peak intensities than the non-irradiated samples, suggesting changes in their diffraction response that may be associated with variations in crystallinity or preferred crystallographic orientation. Nevertheless, the reduction in peak intensity alone is insufficient to confirm a decrease in crystallinity without quantitative analysis of the XRD patterns.

For irradiated marble, the calcite diffraction peak at 2θ = 29.64° exhibited the largest reduction in intensity (81%), followed by decreases of 71.7%, 70.8%, and 53.8%, for the peaks at 43.24°, 47.62°, and 48.58°, respectively. In contrast, the dolomite peaks showed smaller changes, with intensity reductions of 64% at 2θ = 56.62° and only 1.1% at 2θ = 36.04°. These results indicate that the diffraction response to gamma irradiation varied between the two crystalline phases and among their respective diffraction peaks.

Under compressive loading, concrete undergoes deformation and develops resistance to failure, behavior that depends on several factors, including aggregate properties, interfacial bonding, and matrix characteristics. Although the mineralogical composition and crystalline structure of the

aggregates may contribute to their mechanical behavior, the relationship between XRD peak intensities and the compressive strength of concrete requires further investigation.

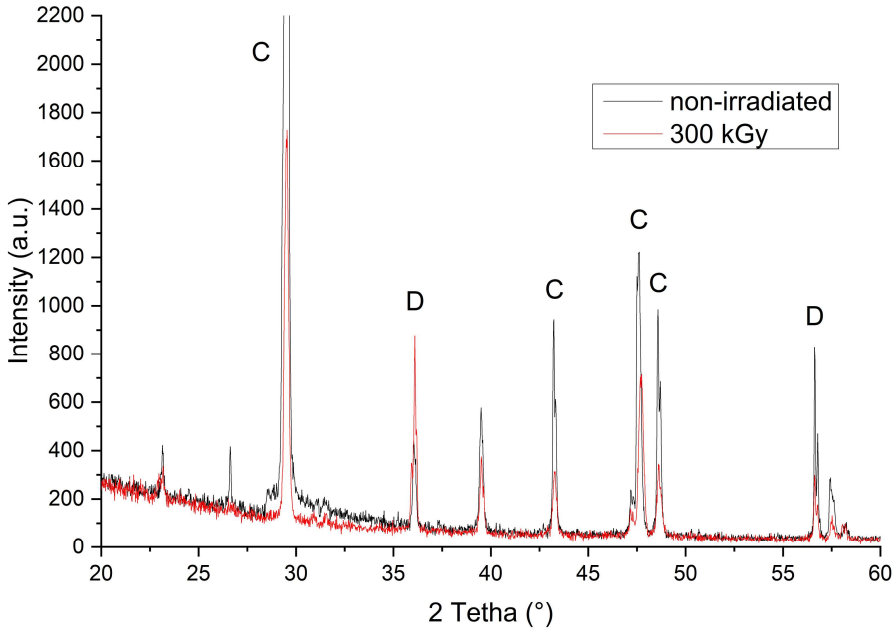


Figure 9. XRD patterns of unirradiated and gamma-irradiated marble.

Figure 10 presents the XRD patterns of non-irradiated and gamma-irradiated mine sand. The most intense diffraction peaks correspond to quartz (SiO_2), labeled Q, at 2θ = 21.9°, 28.56°, 35.54°, and 50.04°. Muscovite [$KA_{l2}(AlSi_3O_{10})(OH)_2$], labeled M, is identified at 2θ = 26.62°. Orthoclase ($AlKO_8Si_3$), labeled O, exhibits peaks at 2θ = 23.66° and 58.76°, whereas albite ($NaAlSi_3O_8$), labeled A, is identified at 2θ = 25.56° and 33.64°. Finally, calcite ($CaCO_3$), labeled as C, is detected at 2θ = 49.7°.

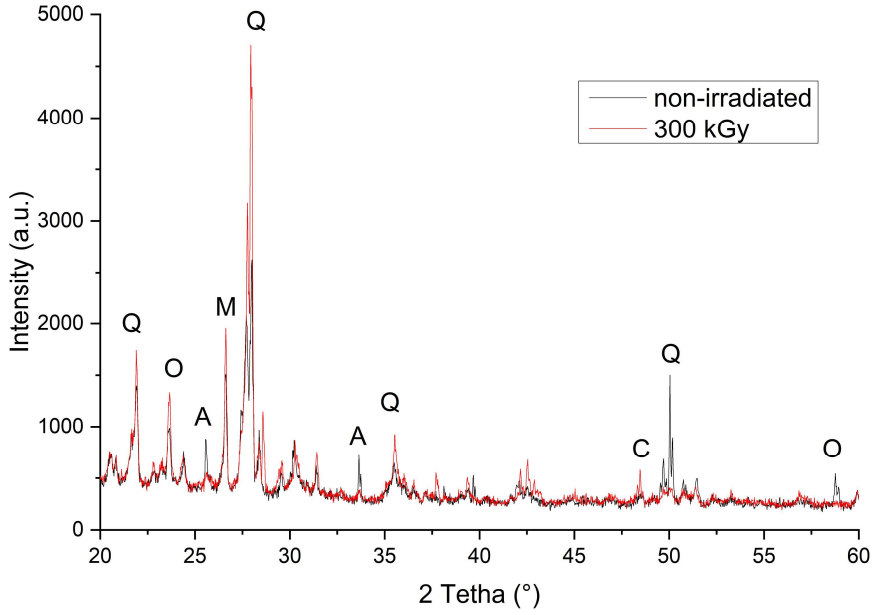


Figure 10. XRD patterns of unirradiated and gamma-irradiated mine sand.

Following gamma irradiation, changes were observed in the intensities of the diffraction peaks for the mineral phases (Figure 11). The peak intensities corresponding to quartz, muscovite, and orthoclase increased, while those for albite and calcite decreased. Quartz exhibited a mixed response: the intensities of some diffraction peaks increased, while others decreased, as illustrated in Figure 11.

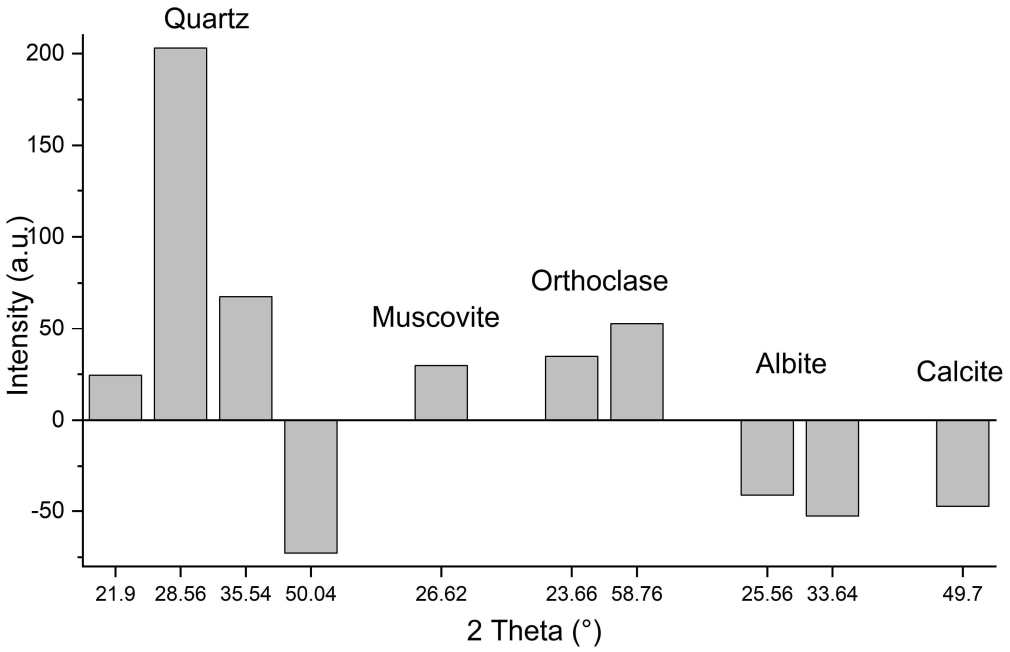


Figure 11. Diffraction peak intensities of mineral phases in gamma-irradiated mine sand.

Figure 12 presents the XRD patterns of non-irradiated and gamma-irradiated ferrochrome slag. Eight intense diffraction peaks were identified, and their positions (2θ) remained unchanged after irradiation, indicating that the crystalline phases were retained. However, changes in peak intensities were observed, suggesting variations in the degree of crystallinity or the relative contributions of the crystalline phases. The identified compounds are described below.

(I) Forsterite (Mg_2SiO_4), labeled F, exhibited its most intense diffraction peaks at 2θ = 22.94°, 35.74°, 36.52°, 39.7°, and 52.26°. Following gamma irradiation, the peak intensities decreased by 22.3%–45.9%.

(II) Spinel ($MgAl_2O_4$), labeled S, were identified by diffraction peaks at 2θ = 32.34°, 39.70°, and 52.26°. After irradiation, their intensities decreased by 22.3%–42.0%.

(III) Chromium spinel [$(Fe,Mg)(Cr,Al)_2O_4$] was identified by a diffraction peak at 2θ = 35.74°, whose intensity decreased by 41.1% following irradiation.

(IV) Enstatite ($MgSiO_3$) was identified by a diffraction peak at 2θ = 32.34°, which exhibited a 42.0% reduction in intensity after irradiation.

Overall, gamma irradiation reduced the intensities of the diffraction peaks associated with the identified crystalline phases, with decreases of up to 45.9%. Although the peak positions remained unchanged, the observed intensity variations suggest that irradiation affected the diffraction response of the material. However, reductions in peak intensity alone do not conclusively demonstrate a decrease in crystallinity, as they may also result from changes in preferred orientation, sample preparation, or measurement conditions. Quantitative assessment of crystallinity would require appropriate peak analysis and normalization.

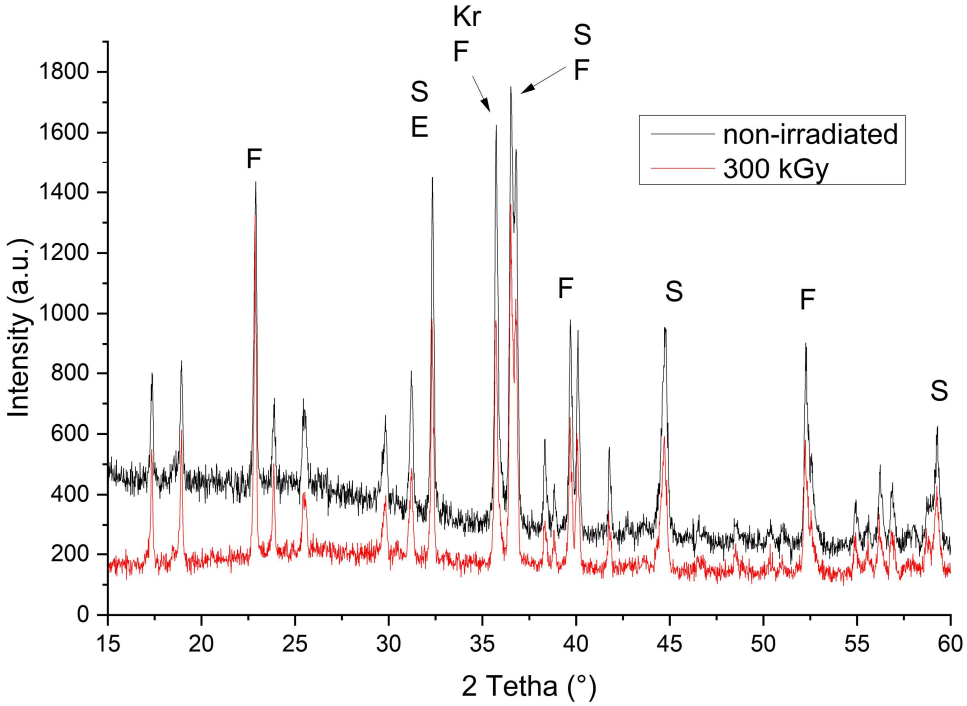


Figure 12. XRD patterns of unirradiated and gamma-irradiated ferrochrome slag.

XRD patterns of the irradiated and non-irradiated aggregates showed that the positions of the main diffraction peaks remained unchanged, while variations in peak intensities were observed. In the marble, the main peaks assigned to calcite and dolomite retained their positions after irradiation. The intensities of the identified peaks decreased, while the mine sand showed increases and decreases in peak intensity depending on the phase. The crystalline phases identified in the ferrochrome slag also retained the positions of their main peaks, although their diffraction intensities decreased. These observations indicate that the qualitative XRD analysis did not detect any changes in the main crystalline phases. Therefore, the available results do not enable us to determine whether these are radiation-induced point defects, changes in the crystalline and amorphous fractions, or chemical reactions within the cement matrix.

4. Conclusions

Waste materials such as FeCr slag can be used to enhance the mechanical properties of concrete. In this study, the addition of 30 wt% FeCr slag increased the compressive strength up to 27% in the C-M and by 28% in the C-mS. The contribution of gamma irradiation to the increase in compressive strength was minimal in the C-M, whereas a slight increase of 3.4% was observed in the C-mS. However, when the concretes containing FeCr slag were exposed to a gamma-ray dose of 300 kGy, the compressive strength increased considerably in formulations containing 30 wt% FeCr. Approximate increases of 20% and 11% were recorded for the C-M-F-300 and C-mS-F-300, respectively.

These increases in compressive strength could be correlated with structural and morphological modifications induced in the fine aggregates (marble, mine sand, and ferrochrome slag). In the case of marble, the intensities of the calcite and dolomite diffraction peaks decreased by 81% and 64%, respectively. For mine sand, the response depended on the mineral phase: The peak intensities for

quartz, muscovite, and orthoclase peaks increased, while those of albite and calcite decreased. In the case of ferrochrome slag, all identified crystalline phases showed reductions in diffraction peak intensity, ranging from 22.3% to 45.9%, which can be correlated with a decrease in crystallinity following irradiation. Another relevant aspect concerns the concentrations of iron and chromium detected in the concrete samples. In the concrete containing marble, gamma irradiation caused a 49% decrease in iron concentration and a 20.4% decrease in the chromium concentration. Conversely, in concrete containing ferrochrome slag, the iron concentration increased by 18%, while no chromium was detected. These results suggest that gamma irradiation could influence the crystalline structure and elemental composition of the concrete components and could contribute to the observed increases in compressive strength.

Although changes in compressive strength and microstructural characteristics were observed under the experimental conditions employed, we did not evaluate electricity consumption, irradiation costs, processing yield, industrial-scale feasibility, or life-cycle environmental impacts. Consequently, the observed mechanical changes should not be interpreted as evidence that gamma irradiation is an economically competitive, energy-efficient, or environmentally beneficial method for strengthening concrete.

Use of AI tools declaration

The authors declare they have not used Artificial Intelligence (AI) tools in the creation of this article.

Acknowledgments

The authors thank the Secretariat of Science, Humanities, Technology and Innovation (SECIHTI, Mexico) for the postgraduate scholarships awarded to J.O. Camacho-Gutiérrez and C. Castro-López.

Author contributions

Conceptualization: Gonzalo Martínez-Barrera, Miguel Martínez-López and Víctor Varela-Guerrero; methodology: Gonzalo Martínez-Barrera, Miguel Martínez-López and Cynthia Castro-López; validation: Gonzalo Martínez-Barrera and Miguel Martínez-López; formal analysis: Gonzalo Martínez-Barrera and Miguel Martínez-López; investigation: Gonzalo Martínez-Barrera, Miguel Martínez-López, and Víctor Varela-Guerrero; data curation: Gonzalo Martínez-Barrera, Joel Olaf Camacho-Gutiérrez, and Cynthia Castro-López; writing—original draft preparation: Gonzalo Martínez-Barrera, and Miguel Martínez-López; writing—review and editing: Gonzalo Martínez-Barrera, Miguel Martínez-López and Víctor Varela-Guerrero; project administration: Gonzalo Martínez-Barrera. All authors have read and agreed to the published version of the manuscript.

Conflict of interest

The authors declare no conflict of interest.

References

1. Islam MZ, Sohel KMA, Al-Jabri K, et al. (2021) Properties of concrete with ferrochrome slag as a fine aggregate at elevated temperatures. *Case Stud Constr Mater* 15: e00599. https://doi.org/10.1016/j.cscm.2021.e00599
2. Gencel O, Koksal F, Ozel C, et al. (2012) Combined effects of fly ash and waste ferrochromium on properties of concrete. *Constr Build Mater* 29: 633–640. https://doi.org/10.1016/j.conbuildmat.2011.11.026
3. Zelić J (2005) Properties of concrete pavements prepared with ferrochromium slag as concrete aggregate. *Cem Concr Res* 35: 2340–2349. https://doi.org/10.1016/j.cemconres.2004.11.019
4. Panda CR, Mishra KK, Panda KC, et al. (2013) Environmental and technical assessment of ferrochrome slag as concrete aggregate material. *Constr Build Mater* 49: 262–271. https://doi.org/10.1016/j.conbuildmat.2013.08.002
5. Yaragal SC, Chethan KB, Jitin C (2020) Durability studies on ferrochrome slag as coarse aggregate in sustainable alkali activated slag/fly ash based concretes. *Sustain Mater Technol* 23: e00137. https://doi.org/10.1016/j.susmat.2019.e00137
6. Jena S, Panigrahi R (2019) Performance assessment of geopolymer concrete with partial replacement of ferrochrome slag as coarse aggregate. *Constr Build Mater* 220: 525–537. https://doi.org/10.1016/j.conbuildmat.2019.06.045
7. Jena S, Panigrahi R (2021) Feasibility study of the properties of geopolymer concrete with ferrochrome slag and silica fume. *Mater Today Proc* 38: 2476–2480. https://doi.org/10.1016/j.matpr.2020.07.510
8. Dash MK, Patro SK (2018) Effects of water cooled ferrochrome slag as fine aggregate on the properties of concrete. *Constr Build Mater* 177: 457–466. https://doi.org/10.1016/j.conbuildmat.2018.05.079
9. Al-Jabri K, Shoukry H (2018) Influence of nano metakaolin on thermo-physical, mechanical and microstructural properties of high-volume ferrochrome slag mortar. *Constr Build Mater* 177: 210–221. https://doi.org/10.1016/j.conbuildmat.2018.05.125
10. Kumar BC, Yaragal SC, Das BB (2020) Ferrochrome ash—Its usage potential in alkali activated slag mortars. *J Clean Prod* 257: 120577. https://doi.org/10.1016/j.jclepro.2020.120577
11. Zhu Y, Rong Z, Shi J, et al. (2026) Low-carbon and low-shrinkage UHPC manufactured with ferrochrome slag by synergistic regulation of binder components and structural build-up rate. *Constr Build Mater* 521: 146049. https://doi.org/10.1016/j.conbuildmat.2026.146049
12. Satpathy L, Parhi SK, Patro SK, et al. (2026) Experimental and SEM image segmentation analysis to establish the optimum content of ferrochrome slag aggregate in lime activated high-volume GGBS-based concrete. *Constr Build Mater* 519: 145835. https://doi.org/10.1016/j.conbuildmat.2026.145835
13. George ES, Hari R, Madhavan MK (2024) Performance assessment of blended self-compacting concrete with ferrochrome slag as fine aggregate using functional ANOVA. *J Build Eng* 89: 109390. https://doi.org/10.1016/j.jobe.2024.109390
14. Polat H, Özel C (2024) Investigation of ferrochrome slag utilization in wet mix shotcrete: Mechanical strength and radiation shielding performance. *Radiat Phys Chem* 223: 111963. https://doi.org/10.1016/j.radphyschem.2024.111963

15. Guan Q, Zhou Y (2025) Utilizing ferrochrome slag and autoclaved artificial aggregates for eco-friendly and economical ultra-high-performance concrete: Mechanical performance and shrinkage control. *Case Stud Constr Mat* 22: e04234. https://doi.org/10.1016/j.cscm.2025.e04234
16. Gencel O, Sutcu M, Erdogmus E, et al. (2013) Properties of bricks with waste ferrochromium slag and zeolite. *J Clean Prod* 59: 111–119. https://doi.org/10.1016/j.jclepro.2013.06.055
17. Yılmaz A, Karaşahin M (2010) Mechanical properties of ferrochromium slag in granular layers of flexible pavements. *Mater Struct* 43: 309–317. https://doi.org/10.1617/s11527-009-9490-2
18. Maruyama I, Ishikawa S, Yasukouchi J, et al. (2018) Impact of gamma-ray irradiation on hardened white Portland cement pastes exposed to atmosphere. *Cem Concr Res* 108: 59–71. https://doi.org/10.1016/j.cemconres.2018.03.005
19. Bouniol P, Aspart A (1998) Disappearance of oxygen in concrete under irradiation: The role of peroxides in radiolysis. *Cem Concr Res* 28: 1669–1681. https://doi.org/10.1016/S0008-8846(98)00138-0
20. Lagomacini JC, Bravo D, León M, et. al (2011) EPR study of gamma and neutron irradiation effects on KU1, KS-4V and Infrasil 301 silica glasses. *J Nucl Mater* 417: 802–805. https://10.1016/j.jnucmat.2010.12.144
21. Khmurovska Y, Stemberk P, Sikorin S, et al. (2021) Effects of gamma-ray irradiation on hardened cement mortar. *Internat J Concr Struct Mater* 15: 17. https://doi.org/10.1186/s40069-020-00452-7
22. Reches Y (2019) A multi-scale review of the effects of gamma radiation on concrete. *Results Mater* 2: 100039. https://doi.org/10.1016/j.rinma.2019.100039
23. Park K, Kim HT, Kwon TH, et al. (2016) Effect of neutron irradiation on response of reinforced concrete members for nuclear power plants. *Nucl Eng Des* 310: 15–26. https://10.1016/j.nucengdes.2016.09.034
24. Cay VV, Sutcu M, Gencel O, et al. (2014) Neutron radiation tests about FeCr slag and natural zeolite loaded brick samples. *Sci Technol Nucl Install* 2014: 971490. https://doi.org/10.1155/2014/971490
25. Korkut T, Gencel O, Kam E, et al. (2013) X-ray, gamma, and neutron radiation tests on epoxy-ferrochromium slag composites by experiments and Monte Carlo simulations. *Int J Polym Anal Charact* 18: 224–231. https://doi.org/10.1080/1023666X.2013.755658



AIMS Press

© 2026 the Author(s), licensee AIMS Press. This is an open access article distributed under the terms of the Creative Commons Attribution License (https://creativecommons.org/licenses/by/4.0)